Atmos. Chem. Phys. Discuss., 11, 4355–4398, 2011
www.atmos-chem-phys-discuss.net/11/4355/2011/
doi:10.5194/acpd-11-4355-2011

Atmospheric Chemistry and Physics Discussions

The impact of temperature changes on summer time ozone and its' precursors in the Eastern Mediterranean

U. Im[1], K. Markakis[2], A. Poupkou[2], D. Melas[2], A. Unal[4], E. Gerasopoulos[3], N. Daskalakis[1], and M. Kanakidou[1]

[1]Environmental Chemical Processes Laboratory (ECPL), Department of Chemistry, University of Crete, Heraklion, Greece
[2]Aristotle University of Thessaloniki, Department of Physics, Laboratory of Atmospheric Physics, Thessaloniki, Greece
[3]Institute for Environmental Research and Sustainable Development, National Observatory of Athens, Athens, Greece
[4]Istanbul Technical University, Eurasia Institute of Earth Sciences, Istanbul, Turkey

Received: 13 December 2010 – Accepted: 24 January 2011 – Published: 7 February 2011

Correspondence to: M. Kanakidou (mariak@chemistry.uoc.gr)

Published by Copernicus Publications on behalf of the European Geosciences Union.

Abstract

Changes in temperature due to variability in meteorology and climate change are expected to significantly impact atmospheric composition. The Mediterranean is a climate sensitive region and includes megacities like Istanbul and large urban agglomerations such as Athens. The effect of temperature changes on gaseous air pollutant levels and the atmospheric processes that are controlling them in the Eastern Mediterranean are here investigated. The WRF/CMAQ mesoscale modeling system is used, coupled with the MEGAN model for the processing of biogenic volatile organic compound emissions. A set of temperature perturbations (spanning from 1 to 5 K) is applied on a base case simulation corresponding to July 2004. The results indicate that the Eastern Mediterranean basin acts as a reservoir of pollutants and their precursor emissions from large urban agglomerations. During summer, chemistry is a major sink at these urban areas near the surface, and a minor contributor at downwind areas. On average, the atmospheric processes are more effective within the first 1000 m. The response rate of biogenic emissions to temperature changes is calculated to be 9±3% K^{-1}. Ozone concentrations respond almost linearly to the changes in the ambient temperature with rates of 1±0.1 ppb O_3 K^{-1} for all studied urban and receptor stations except for Istanbul, where a 0.4±0.1 ppb O_3 K^{-1} change rate is calculated, which is almost half of the domain-averaged increase of 0.9±0.1 ppb O_3 K^{-1}. The computed changes in atmospheric processes are also linearly related with temperature changes.

1 Introduction

The contributions of natural and anthropogenic sources on emissions and thus, air quality levels, vary depending on geography and seasonality. Biogenic emissions from vegetation can affect the gas-phase chemistry, as well as the formation of secondary organic aerosol (SOA) formation (Kanakidou et al., 2000). Wind-driven dust and sea-salt emissions also contribute to aerosol concentrations (Athanasopoulou et al., 2008).

ACPD
11, 4355–4398, 2011

Changes in climate can impact air quality in various manners, including changes in temperature, precipitation and atmospheric ventilation (Jacob and Winner, 2009). Ozone (O_3) is a product of complex non-linear interactions between nitrogen oxides (NO_x) and volatile organic compounds (VOC), in presence of sunlight (Crutzen, 1994; Seinfeld and Pandis, 1998). Depending on VOC/NO_x ratios, O_3 can be produced or consumed (Sillman and Samson, 1995). Biogenic emissions of isoprene increase with increasing temperature, affect SOA formation and can enhance O_3 concentrations depending on NO_x availability. Recent studies indicate that temperature, among other meteorological variables, has the largest effect on O_3 concentrations (Sanchez-Ccoyllo et al., 2006; Dawson et al., 2007).

The Eastern Mediterranean basin acts as a receptor of anthropogenic emissions from Europe, wind-driven dust from Sahara desert (Kanakidou et al., 2007 and 2011), biogenic hydrocarbons from the surrounding vegetation (Liakakou et al., 2007) and sea-salt particles (Athanasopoulou et al., 2008). In addition, there are two important megacities: Istanbul (~12 million inhabitants) and Cairo (~16 million inhabitants), as well as the large urban agglomerations like Athens (~4 million inhabitants), contributing to the anthropogenic emissions in the region. The result is complex photochemistry and transport patterns leading to elevated levels of O_3 and particulate matter (PM) in the area (Kanakidou et al., 2011; Gerasopoulos et al., 2006a, b). Ground observations and satellite measurements show elevated amounts of O_3 over the Eastern Mediterranean during the last decade (Vrekoussis et al., 2007). Gerasopoulos et al. (2005) reported high background O_3, particularly in spring and summer, attributed to meteorological conditions. Observations showed that while primary pollutant levels decrease downwind, secondary pollutants like O_3 are produced photochemically during transport of precursors from the surrounding regions: Europe, Balkans and north of the Black Sea. Pollution transported toward the Mediterranean is affected by local meteorological parameters like land-sea breeze circulations and orographic flows (Lelieveld et al., 2002). In addition to the near-surface long range transport (LRT) of pollutants, the high O_3 concentrations in the planetary boundary layer (PBL) are, partly attributed to entrainment

ACPD
11, 4355–4398, 2011

from the free-troposphere. These pollution patterns have been observationally documented by several experimental studies; however the number of mesoscale modeling studies focusing on this area remains limited.

Chemistry and transport models (CTMs) can serve as fundamental tools to understand the complex and dynamic interactions between meteorology and chemistry at multiple temporal and spatial scales (Kindap et al., 2006; Kallos et al., 2007; Im et al., 2010). Earlier modeling studies for the region pointed out the importance of local and regional circulations on air pollutant levels (Melas et al., 1998a and b). Poupkou et al. (2008) showed that the Athens urban plume significantly impacts the O_3 levels over the southern Aegean and Mediterranean. Lazaridis et al. (2005) applied the UAM-AERO model to simulate photo-oxidants and PM in the Eastern Mediterranean and indicated the importance of photo-oxidant and fine aerosols dynamics in the area as well as the significant contribution of regional transport to the observed pollution levels. Vegetation is a strong source of VOC emissions in the Mediterranean (Symeonidis et al., 2008). Poupkou et al. (2006) found that the biogenic emissions can lead to an increase of mean O_3 levels up to 10 ppb in Greece during summer while their impact on mean maximum ozone values is more pronounced leading to increases that can reach 20 ppb. Similar results for the Eastern Mediterranean are reported by Curci et al. (2009) modeling study for Europe. Recently, Im et al. (2011) evaluated a larger impact of biogenic emissions on the regional O_3 levels that can reach 25 ppb in the extended Istanbul area. These results demonstrate the importance of natural emissions on O_3 levels in the area. CTMs can also provide useful information on how changing meteorology may affect the pollutant concentrations (Tsigaridis et al., 2005; Dawson et al., 2007; Liao et al., 2009) as well as the physical and chemical processes leading to these concentration changes (Hogrefe et al., 2005; Goncavles et al., 2008), by employing scenarios that have perturbed meteorology and/or emissions.

The Mediterranean is a very sensitive region to changes in climate (IPCC, 2007). Thus, future changes in climate and local meteorology can have significant impacts on the natural emissions and regional air quality. In the present study, we investigate

ACPD
11, 4355–4398, 2011

the potential impacts of increases in ambient temperature on air quality in the Eastern Mediterranean. We focus on the levels of O_3 and its precursors from 1–15 July, 2004. For this purpose, the US EPA Community Multiscale Air Quality (CMAQ) chemistry and transport model driven by the Weather Research and Forecasting model (WRF-ARW) deduced meteorology is used and a number of temperature perturbation scenarios are performed. The contributions of various atmospheric processes within the surface layer and the PBL are analyzed. Focus is put on the effects of temperature changes on the biogenic emissions, photochemistry, and the atmospheric processes.

2 Materials and methods

2.1 Meteorological model

In order to produce the meteorological fields necessary for the CMAQ model, WRF-ARW v3.1.1 has been used (Sharmock and Klemp, 2008). The WRF model is widely used by the mesoscale modeling community and has proven to give satisfactory results for the Mediterranean region (Borge et al., 2008; Im et al., 2010). The initial and boundary conditions have been provided from the National Centers for Environmental Prediction (NCEP) on $1^{\circ}\times1^{\circ}$ resolution. The simulations have been carried out on a single domain that covers the Eastern Mediterranean region on a 30 km spatial resolution (Fig. 1). The domain has 58 and 47 grid cells on east-west and north-south directions, respectively, with 30 vertical layers extending from 8 m on surface to ~16 km on domain top. The physical options used in this study are WRF Single Moment 6-class microphysics scheme (Hong and Lim, 2006), RRTM (rapid radiative transfer model) longwave radiation scheme (Mlawer et al., 1997), Dudhia shortwave radiation scheme (Dudhia, 1989), NOAH land surface model (Chen and Dudhia, 2001), Yonsei University Planetary Boundary Layer scheme (Hong et al., 2006) and Kain-Fritsch cumulus parameterization scheme (Kain, 2004). Additionally, analysis nudging has been performed on temperature, wind and moisture parameters.

ACPD
11, 4355–4398, 2011

2.2 Emissions

The emission inventory used here is a compilation of different smaller scale emission inventories. The most important anthropogenic emission sectors in Greece as well as in the large urban agglomerations of Athens, Greece and Istanbul, Turkey have been quantified using real activity information as well as high resolution digital maps utilizing bottom-up methodologies.

The emission inventories for all anthropogenic sources have been originally compiled in 10 km resolution for Greece and in 2 km resolution for Athens (Markakis et al. 2010a, b). These inventories have been mainly based on the bottom-up approach using activity information and statistics for traffic loads in major roads, fuel consumptions of vehicles, off-road vehicles, various ship types, and stack measurements in industries. The remainder of the domain shown in Fig. 1a is covered by the emission inventory of French National Institute for Industrial Environment and Risks (INERIS) (https://wiki.met.no/cityzen/page2/emissions). This inventory is a re-gridded product of the emissions of the European Monitoring and Evaluation Programme (EMEP) database (http://www.ceip.at/). Emissions within each $0.5^{\circ} \times 0.5^{\circ}$ EMEP grid cell have been reallocated to a $0.1^{\circ} \times 0.1^{\circ}$ lon/lat grid using the high resolution (300 m) global land cover database of GlobCover (http://ionia1.esrin.esa.int/).

The Istanbul inventory (Im, 2009; Im et al., 2010) is the first high resolution emission inventory developed for the city (2 km resolution) and covers gridded and hourly resolved emission rates for carbon monoxide (CO), NO_x, sulfur oxides (SO_x), ammonium (NH_3), non-methane VOCs (NMVOC) and particulate matter (PM_{10} and $PM_{2.5}$). Emissions for a number of sources such as road transport, industrial and residential combustion and cargo shipping are calculated based on detailed information gathered from official sources of the municipality of Istanbul.

ACPD
11, 4355–4398, 2011

Finally the abovementioned individual emission inventories have been merged in order to meet the needs of this study for a 30 km resolution grid. All PM and NMVOC species are speciated into Carbon Bond 5 (CB5) species (Yardwood et al., 2005). The vertical distribution of emissions is calculated based on the Selected Nomenclature for Air Pollution (SNAP) codes provided by Simpson et al. (2003). NO_x emissions summed over all the sectors and averaged over the studied period is presented in Fig. 1a. Figure 1a clearly depicts the elevated emissions over Istanbul and Athens. The shipping routes also stand out, pointing to a potentially significant environmental impact of ship emissions in the region. The mean diurnal variability of the emissions over the model domain is shown in Fig. 1b that demonstrates the clear peaks in the morning and evening rush hours, which are dominated by the road-traffic sector.

The biogenic emissions have been calculated using the Model of Emissions of Gases and Aerosols from Nature (MEGAN) module of the WRF-CHEM 3.1.1 online-coupled meteorology-chemistry model (Grell et al., 2005). Detailed description of the MEGAN model is provided in Guenther et al. (2006). This online version of MEGAN in WRF-CHEM model uses the same methodology with the offline version of MEGAN model 2.04 (Qian et al., 2010). MEGAN calculates 134 biogenic species, which are then mapped to 20 major groups, including isoprene, monoterpenes, sesquiterpenes, oxygenated compounds, and other VOCs from terrestrial vegetation and nitrogen oxide from soils. CO emissions are also estimated by the model. The input files needed to run the MEGAN model include modified emission factors, satellite-derived vegetative cover, including Leaf Area Index (LAI) and Plant Functional Type (PFT) fractions, as well as climatological temperature and solar radiation for each grid cell. The WRF-CHEM model is modified to calculate all 20 MEGAN biogenic emission rates for each time step of the meteorology simulation. The emission rates are then converted to CB5 chemical species in order to be merged with the anthropogenic emissions for use in the CTM simulations. Mapping of individual NMVOCs to CB5 species has been based on the assignment matrixes and molecular weights described in Yardwood et al. (1999, 2005).

ACPD
11, 4355–4398, 2011

2.3 Chemistry and transport model

The CMAQ model version 4.7 has been used to simulate the atmospheric transport and the chemistry of the pollutants (Byun and Schere, 2006). CMAQ is a widely used model to simulate the atmospheric composition (Hogrefe et al., 2001; Unal et al., 2005; Kindap et al., 2006; Odman et al., 2007; Im et al., 2010). The boundary and initial conditions have been extracted from the Transport Model version 4 (TM4-ECPL) global chemistry and transport model (Myriokefalitakis et al., 2008, 2010 and 2011), which is able to simulate gas phase chemistry coupled with all major aerosol components including secondary, sulfate, nitrate and organic aerosols. The TM4-ECPL species have been then mapped in to CB5 species to be consistent with the other chemical input data, using the assignment factors described in Yardwood et al. (2005). AERO5 module has been employed as the aerosol mechanism. This module also calculates sea-salt emission fluxes based on land-sea fractions in each grid cell, along with wind speed and relative humidity (Gong, 2003; Zhang et al., 2005). Yamartino scheme for advection (Yamartino, 1993) and asymmetric convective model (ACM2) scheme (Pleim, 2007) for vertical diffusion have been used in the study. The aqueous cloud chemistry has also been accounted for the simulations (Foley et al., 2010).

Integrated Process Analysis (IPR) tool of the CMAQ system has been employed to identify the dominant physical processes for 3 species/groups (O_3, NMVOCs and NO_x), at the surface (first model layer extending up to 8 m) and in the whole PBL, which extends up to ~2.6 km that corresponds to the first 27 layers, varying spatially and temporally. IPR analysis applications have been reported in the literature characterizing episodic events (San Jose et al., 2002; Goncavles et al., 2009) as well as long-term (Zhang et al., 2006) and climatological simulations (Hogrefe et al., 2005). The atmospheric processes examined in IPR are horizontal and vertical transport, emissions of primary species, gas-phase chemistry, dry deposition, cloud processes and aerosol processes. Transport is calculated as the sum of advection and diffusion, horizontally (HTRA) and vertically (VTRA). Aerosol processes (AERO) include the effect of particle

ACPD
11, 4355–4398, 2011

formation, condensation, coagulation and aerosol thermodynamics. Cloud processes (CLDS) are defined as the net effect of aqueous chemistry, below- and in-cloud mixing, cloud scavenging, and wet deposition. The weighted contributions of each process on O_3, NO_x and VOC levels have been estimated using Eq. (1), where$\%PC_i$ is the relative contribution of the process i on the species, PC_i is the individual contribution of that process (P), and PC_j is the contribution of each process, j, affecting the species levels in the atmosphere (Goncalves et al., 2009).

$$\%PC_i = \frac{PC_i}{\sum_j \text{abs}(PC_j)} \times 100 \quad (1)$$

In the present study, we evaluate the major atmospheric processes (PC_j): HTRA, VTRA, DDEP, and CHEM that determine O_3 concentrations.

2.4 Simulations

A number of scenarios have been simulated in order to evaluate the model system performance and the response of isoprene emissions, O_3 and its precursor's concentrations to temperature changes in the Eastern Mediterranean. All simulations have been conducted for a 15-days period between July 1 and July 15, 2004. The period was chosen based on the availability of isoprene measurements at the Finokalia air quality station in Crete. A spin-up period of 11 days has been used starting from 20th of June, 2004. The model results from this period have not been used in the model evaluations.

1. The base case simulation (S0) has been conducted using the corresponding June and July 2004 meteorology.

2. Scenario S1 has been applied to estimate the possible impact of a homogenous increase of air temperature by 1 °K in the whole domain, both horizontally and vertically. This has been achieved in two steps: first, the MEGAN code was modified so that for each time step when the biogenic emissions are calculated, the

ACPD
11, 4355–4398, 2011

surface temperature is increased by 1 °K compared to the temperatures in S0. Second, the Meteorology-Chemistry Interface Processor (MCIP: Otte and Pleim, 2010) outputs, which are used as the meteorological inputs for the CMAQ model, are modified to have increased temperatures by 1 °K throughout the modeling domain.

3. Scenario S2: same as S1 but for a 2 °K increase.
4. Scenario S3: same as S1 but for a 3 °K increase.
5. Scenario S4: same as S1 but for a 4 °K increase.
6. Scenario S5: same as S1 but for a 5 °K increase.
7. Scenario S6 has been used to investigate the impact of a realistic temperature field from a warmer year on the chemical composition in the area. For this purpose, the temperature field of the S0 scenario has been replaced by the temperature field of the year 2007. The replacement has been conducted at the NCEP input data to the WRF model. This enabled the simulation of the impact of this temperature change to the meteorological fields driving atmospheric transport and chemistry in the CMAQ model and to the biogenic emissions. Figure S1 in the supplementary materials shows the difference of the new temperature fields of each scenario from the base scenario, averaged over the domain at each model layer.

2.5 Model performance metrics

The model performance has been analyzed by comparison of the model results with observations from various locations in the model domain. A number of statistical parameters have been calculated to serve as metrics for the quantification of the model success in simulating the observations on daily basis. The statistical

ACPD
11, 4355–4398, 2011

parameters applied are correlation coefficient (r), Mean Normalized Bias (MNB) and Index of Agreement (IOA). More information is provided in the supplementary material.

Isoprene observations at Finokalia, Greece (University of Crete monitoring station; Mihalopoulos et al., 1997) during summer 2004 (Liakakou et al., 2007) have been used to evaluate isoprene simulations in the model. In addition, O_3 simulations have been evaluated using observations at Finokalia (Liakakou et al., 2007), Sarachane monitoring station from the Air Quality Network of Istanbul Metropolitan Municipality (http://www.havaizleme.gov.tr/Default.htm), from the National Air Pollution Monitoring Network of the Hellenic Ministry of Environment Energy and Climate Change for Athens, and finally for Thessaloniki from the Air Quality Monitoring Network of the Region of Central Macedonia. These stations have then been grouped according to their locations in the model domain and the comparisons of model results and observations have been done using the averages of the rural stations that fall into the same group. Urban core stations have not been included because the resolution of the model is not fine enough to resolve spatially highly variable surface emissions. Based on the classification, 5 station groups are generated (see Table 1).

3 Results and discussion

3.1 Model evaluation

The model calculated isoprene and terpene (monoterpenes and sesquiterpenes) emissions, summed over the 15-day simulation period are presented in Fig. 2. The south western parts of Greece, Turkey, and the Black Sea are characterized by relatively high isoprene and terpene emissions. For the 15-day simulation period, the model calculated domain-wide isoprene emissions of 177 tons largely exceed those of monoterpene (49 tons) and sesquiterpene (4 tons). α- and β-pinenes are calculated to be the major monoterpene species (57%). β-caryophyllene contribute by 60% to the total sesquiterpene emissions. Note however that uncertainties of a factor of 3–5 are

ACPD
11, 4355–4398, 2011

associated with the biogenic emission estimates (Simpson et al., 1999; Smiatek and Steinbrecher, 2006; NATAIR, 2007). These uncertainties may originate from a number of sources including the plant-specific emission potentials, the vegetation type and the associated biomass, and the impact of various climate parameters like temperature, radiation, humidity and greenhouse gases, and chemical processes that determine the emissions of VOC in the canopy (Guenther et al., 2006; Arneth et al., 2007; Poupkou et al., 2010). For July 2003, Steinbrecher et al. (2009) used different modeling approaches in order to estimate the biogenic emissions over Europe and calculated differences of a factor of 1.3 for the isoprene emissions and a factor of 3.3 for the terpene emissions. For the same period, Poupkou et al. (2010) found a good agreement in total isoprene emissions (a factor of 1.2) between the Biogenic Emission Model (BEM) and the MEGAN model (Guenther et al., 2006).

Due to the above-mentioned high uncertainties in biogenic emissions, simulated isoprene concentrations may also differ significantly from observations, particularly in remote regions such as Finokalia, which represents a background station in the Eastern Mediterranean. Earlier studies for the Eastern Mediterranean including comparison between observed and simulated isoprene concentrations are very limited. Poupkou et al. (2010) applied the BEM model coupled with the CAMx chemistry and transport model (ENVIRON, 2006) for Europe in 30 km spatial resolution for the summer in 2003. They evaluated BEM/CAMx calculated isoprene concentrations with the available EMEP network data and found agreement within a factor of 2–4, depending on location. In our study, the WRF-MEGAN/CMAQ model (S0) overestimates the isoprene concentrations at Finokalia by a factor of 2 (91%), which results in a low IOA value of 0.3 (Table 2). The isoprene temporal variation is captured moderately with a correlation coefficient of 0.5 (Fig. 3, Table 2). Although there are missing days of observations for which the model calculated isoprene concentrations show a sharp increase, the good agreement of the model calculated temperatures with observations ($r = 0.8$; not shown here) suggests comparable isoprene concentrations for these days.

ACPD
11, 4355–4398, 2011

In the present study, the temporal variation of daily mean O_3 concentrations calculated by the CMAQ model agree moderately with observations from FIN and THES and much better with IST and ATH station groups (Table 2). Figure 4 shows the comparison of calculated daily mean O_3 concentrations with available observations at all station groups. Particularly in groups IST and ATH2, temporal variability is successfully reproduced ($r = 0.9$). On the other hand, the concentrations are overestimated at all stations, ranging from 7.4% (THES) to 47.9% (FIN). These differences can be attributed to many sources of uncertainties, particularly the emissions and their spatial resolution that imply a potentially underestimated O_3 titration by reactions with NO_x. In addition, isoprene concentrations are overestimated by a factor of 2 at FIN, which also has an impact on the O_3 production. The overestimation of O_3 at FIN can be partially due to underestimated O_3 removal through dry deposition within the corresponding grid cell that is covered largely by water. The better performance of the model (IOA = 0.9) for the Istanbul region is attributed to the updated high resolution anthropogenic emissions inventory developed recently for Istanbul and adopted here (Im, 2009).

The mean surface distributions of O_3, NO_x, CO and OH concentrations and the molar VOC/NO_x ratios are presented in Fig. 5. The relatively low O_3 concentrations in Istanbul (19 ppb) and Athens (35 ppb) are due to the O_3-titration by NO_x taking place in these two big agglomerations, which is clearly seen in the figure. The impact of the Athens urban plume on the southern Aegean Sea air quality (Fig. 5a) is demonstrated in agreement with the findings of Poupkou et al. (2009). It is also clear that shipping emissions are an important anthropogenic source of NO_x in the region (Fig. 5b), in agreement with earlier studies in the region (Athanasopoulou et al., 2008). Poupkou et al. (2008) calculated the maritime transport emissions contribution at approximately 20 ppb on the coastlines of southern and western Greece, while in the regions influenced by high amounts of nitrogen oxides emitted from the sea transport activities, the O_3 concentrations were suppressed. On the other hand, due to the higher NMVOC and lower NO_x emissions in Athens (annually 93 and 78 ktons, respectively: Markakis et al., 2010a), than in Istanbul (annually 77 and 305 ktons, respectively: Im, 2009),

ACPD
11, 4355–4398, 2011

higher VOC/NO_x ratio and O_3 concentrations are calculated in Athens (Fig. 5e). The OH distribution indicates a higher oxidative capacity of the Athens atmosphere than over Istanbul. This can be attributed both to higher NMVOC emissions that result in more organic compounds in the atmosphere and to faster reaction rates due to warmer temperatures over Athens, overall leading to more intensive photochemical activity.

The model calculated molar CO/NO_x ratios are compared with the observations from measurement networks at IST, ATH and THES. The CO/NO_x ratio is an indicator of emission composition and air masses ageing. The surface-mean distribution of CO/NO_x molar ratios are computed for simulation S0 and are depicted in Fig. 5f. The model is able to capture the pattern within the stations, as CO/NO_x ratios increase due to regional influence from below 50 in the large agglomerations to above 150 downwind. The smallest ratio of Istanbul indicates significant local influence whereas in Athens, regional influence is much stronger. Finally, Finokalia has the largest regional influence. The model highly underestimates the CO/NO_x ratio in Istanbul by a factor of 4 (2.9 versus 15.5), whereas in Athens agreement is much better (14.2 versus 14.6). In Istanbul, the large difference can be attributed to the uncertainty in the road-transport emissions. At THES, the model calculated CO/NO_x molar ratio is in very good agreement with the observations with a slight overestimation (24.9 versus 21.2). Due to the lack of observations at FIN for the period, the model calculated ratio is compared with the annual average ratio provided by Kanakidou et al. (2011). At FIN, the model calculated a CO/NO_x ratio of 125 whereas measurements provide values between 100 and 300. The results are also in agreement with the annual observed long-term averages from measurements (Kanakidou et al., 2011 and references therein).

3.2 Process analyses

The IPR analysis calculates the mass concentration fluxes from each atmospheric process that affects the concentration of the individual species. These flux values are then divided by the sum of the absolute values for each process to get the % contribution of the respective process to the total. The present IPR analysis focuses on the relative

ACPD
11, 4355–4398, 2011

contributions of HTRA, VTRA, DDEP and CHEM processes to O_3 concentrations at different vertical levels in PBL. For the whole modeling domain (not shown here), the S0 simulation results show that VTRA is the major source term of surface O_3 (50%) and DDEP is the major sink (48%). HTRA and CHEM have relatively very low contributions to O_3 levels. On the other hand, in the entire PBL, the calculations show that chemistry is a more important source term (7%) than at surface. VTRA is still the major source term (43%) and DDEP the major sink term (29%). HTRA is an important sink of O_3 (21%) when the entire PBL is considered.

The IPR analyses are employed for individual station groups within the surface layer and PBL, as well as each vertical layer within the PBL, in order to better understand the different physical and chemical processes working in the atmospheres of these cities. The overall results for each station group presented in Table 3 show that at the surface layer VTRA is the major source term for all station groups, being lowest in ATH1 (34%) and the highest in ATH2 (50%). At the rest of the station groups, VTRA contributes by more than 40%. DDEP and CHEM are sink terms of O_3 at all station groups. Where chemical destruction of O_3 is dominant, DDEP becomes less pronounced (IST and ATH1). These station groups are located in the emission hot spots and O_3 is titrated rapidly by fresh NO emissions. In the entire PBL, VTRA is still a major source of O_3 in FIN, IST and THES. However, in both ATH station groups, VTRA becomes a sink, suggesting an updraft of the air parcels carrying the pollutants to higher altitudes. At these two station groups, HTRA becomes very effective in the PBL carrying O_3 to the area. CHEM is more pronounced in the PBL than at the surface layer, particularly at the IST station group, where removal through chemical destruction (titration by NO_x) is even higher (−44.7 %) than at the surface layer (−33.8%), and in ATH1. In both ATH station groups, CHEM is a sink at the surface layer and becomes a weak source of O_3 when the entire PBL is considered.

The impact of VTRA is particularly remarkable at the surface layer at all station groups whereas HTRA can be as significant as VTRA within the entire PBL. Since dry deposition occurs at the surface layer only, its contribution is smaller when analyzing

ACPD
11, 4355–4398, 2011

the whole PBL. As presented in Fig. 6, the contributions of all HTRA, VTRA and CHEM are more pronounced in the first ~1000 m above the surface. At FIN, HTRA is a sink term up to around 1000 m, and a source term above 1000 meters. O_3 is transported vertically to FIN within the first 1000 meters and carried away above. At the IST station group, VTRA is a source for O_3 in the first 100 meters. Between 100 and 500 meters, O_3 is carried away from IST and towards higher altitudes; there is removal of O_3 by VTRA. The IST area is a net chemical sink of O_3 throughout the entire PBL. The effect is particularly significant in the first 100-200 meters, where in addition to the domestic combustion, traffic and shipping emissions are extremely effective. O_3 is horizontally transported to both ATH1 and ATH2 station groups. While HTRA is effective in the first 1000 m of PBL over ATH1, O_3 is advected away from ATH2 in the first 20 m and carried towards the station group at higher altitudes.

As presented in Table 3, at all station groups, local emissions (EMIS) are the main sources of NO_x and NMVOCs, whereas VTRA is the dominant sink, different from the case for O_3. HTRA is more effective in the entire PBL compared to the surface layer for both NO_x and NMVOC. DDEP is not an important sink term for these species as it is for O_3. Generally, all station groups are subject to more effective contribution of HTRA in the entire PBL than at the surface layer that results in a relative decrease of VTRA impact on all species.

A snapshot of the horizontal and vertical circulation patterns in the area is given in Fig. 7 that is plotted using the RIP (Read/Interpolate/Plot) program of NCAR Graphics version 4.5. The figure shows the circulation vectors, along with potential temperatures in the two cross-sections. The first cross-section cuts across the Istanbul-Finokalia axis (A–A′) while the second cross-section cuts across Thessaloniki-Athens- Finokalia axis (B–B′) (Fig. 1). As exhibited, in both cross-sections, northerly flow is prevailing in the modeling domain. The horizontal winds are stronger in the A–A′ cross-section which is closer to the axis of the Etesians (Fig. 7a) compared to the B–B′ cross-section (Fig. 7b). In Istanbul (Fig. 7a), the air parcels move upward until around 850 mbar. This pattern is consistent with the existence of the two convective cells driven by the heat

ACPD
11, 4355–4398, 2011

island effect of the megacity, as described in Ezber et al. (2007). The upward motion carries the air pollutants emitted over Istanbul to higher altitudes, facilitating their long distance transport. Although, the updraft is stronger over Athens where it is enhanced by the topography (Fig. 7b), part of the air parcels carrying the cities pollutant emissions are captured in the sea breeze circulation and are transported back to the city (vertical recirculation, Melas et al., 2005). However, some of the air parcels are lifted to higher altitudes from where they can be transported towards south. Polluted air masses finally subside over Crete. It should be noted that a 30 km spatial resolution may not be enough to accurately resolve the local circulations in the area. These results are consistent with previous studies done in the area. Gerasopoulos et al. (2005, 2006b) used 7-year observations of O_3 from Finokalia and found that transport from Europe was the main mechanism that controlled O_3 levels during summer in particular. Similarly, Vrekoussis et al. (2007) showed that northerly transport was a major contributor to nitrate (NO_3) levels, along with O_3, during summer. They have shown that intrusion from the free troposphere and mass transfer in lower altitudes from polluted Europe, were significant sources in the Eastern Mediterranean.

3.3 Scenario analyses

The effect of temperature changes on isoprene emissions is depicted in Fig. 8a. The figure shows a quasi-linear positive response of isoprene emissions to increase in temperature. Domain-wide, increases of ambient temperatures by 1-to-5degrees lead to 9±3% K^{-1} increases in isoprene emissions. Similar pattern is also seen at the individual station groups, varying from 7.4±1.7% K^{-1} at ATH2 to 10.6±4.7% K^{-1} at IST. Table 4 provides the changes in domain-wide biogenic emissions (isoprene, monoterpenes and sesquiterpenes) and ozone, NO_x and VOC concentrations relative to the base case scenario, for the 15-days simulation period. Terpene emissions demonstrate a similar pattern to isoprene emissions, having the largest response to the 2-degrees increase in temperature.

ACPD
11, 4355–4398, 2011

Scenario S6 provides a domain wide decrease of isoprene emissions by 4.1% (Table 4) due to the lower temperatures applied over land compared to S0. However, for the whole domain, an average increase of 0.07 °C exists at the surface. At Finokalia, 10% lower isoprene emissions are calculated compared to S0, whereas higher isoprene emissions are calculated at the other station groups (1.8% to 7.7%). Terpene emissions also decrease in scenario S6.

The increase in isoprene emissions together with enhanced photochemistry due to the higher temperatures result domain wide in higher O_3 concentrations corresponding to a domain-mean O_3 level increase by 0.9±0.1 ppb O_3 K^{-1} (Fig. 8b). All station groups experience a quasi linear positive response to temperature changes for O_3 concentrations; that is 0.4±0.1 ppb O_3 K^{-1} at IST, 1±0.1 ppb O_3 K^{-1} at ATH1, 1.1±0.1 ppb O_3 K^{-1} at ATH2, 0.9±0.1 ppb O_3 K^{-1} at THES and 1.2±0.2 ppb O_3 K^{-1} at FIN. The domain mean VOC/NO_x molar ratio decreases by 0.9±0.3% K^{-1} (Fig. 8c). Regarding the station groups, FIN, ATH1 and ATH2 experience VOC/NO_x ratio decreases by 1.9±0.8, 1.4±0.5 and 2.4±0.7% K^{-1}, respectively; whereas IST and THES station groups have increased VOC/NO_x ratios by 0.4±0.3 and 0.4±0.2% K^{-1}, respectively. PAN concentrations decrease in all simulations and station groups, as well as the whole domain, by 0.03±0.01 ppb K^{-1} on average (Fig. 8d). This change is due to the enhancement of the decomposition of PAN to NO_2, which can then form O_3 and increase the O_3 concentrations (Sillman and Salmon, 1995; Dawson et al., 2007).

In the scenario S6, an increase of domain wide mean O_3 concentrations by 0.42 ppb is calculated. The highest change is calculated at the IST group (+3.6 ppb) whereas for ATH1, the mean O_3 concentrations are enhanced by 1.54 ppb, in ATH2 0.84 ppb and THES 0.97 ppb. At FIN, O_3 levels decrease by 0.05 ppb. The domain-mean molar VOC/NO_x ratio decrease by 3.7%. The smallest effects occur in hotspot areas of IST and ATH1 (0.4 and 4.4%, respectively), whereas other station groups experience larger decreases (−11.8% in FIN, −13.4% in ATH2 and −15.4% in THES). The PAN concentrations also decrease by 0.05 ppb domain wide, whereas Finokalia and IST experience a PAN decrease of 0.04 ppb, ATH1 0.09, ATH2 0.07 and THES 0.08 ppb.

ACPD
11, 4355–4398, 2011

The spatial distributions in changes of isoprene emissions and O_3, VOC/NO_x and PAN concentrations at the surface layer in scenarios S5 and S6 are presented in Fig. 9. This figure clearly shows the large changes in the Athens urban plume in scenario S5 compared to the base case (S0) due to a homogeneous warming in the atmosphere. O the other hand, due to the different temperature fields in the S6 scenario, the changes are more scattered around the domain. The largest changes around the extended Athens area are due to the enhancement of NMVOC emissions by increasing temperatures, thus producing more O_3 downwind.

The impact of a 5 degrees increase of temperatures (S5) on the vertical levels of O_3 at FIN, IST and ATH1 stations is presented in Fig. 10. The figure shows that in emission hot spots of IST and ATH1, there is a significant change of O_3 concentrations with height compared with the downwind site FIN, where the change is less pronounced. This can be attributed particularly to the intensity of the traffic emissions close to the surface over the urban sites where they destroy ozone. The impact over IST is larger than over ATH1 due to the very large NO_x emissions. The O_3 concentrations become very similar (~72 ppb) around 4000 m at all stations, indicating an increased free-tropospheric O_3 background over the entire region. The difference in simulated O_3 concentrations between scenarios S5 and S0, averaged over the PBL is calculated to be 5.1 ppb for FIN, 3.6 ppb for IST and 5.3 ppb for ATH1. However, as seen in Fig. 10, these changes are not uniform throughout the vertical extend of the model.

Figure 11 shows the budget term responses of surface and PBL O_3 in the model domain and at IST, ATH1 and FIN for each scenario. At the surface layer and for the model domain (Fig. 11a), the changes in the mass fluxes associated with various processes for the different scenarios are almost linear with the temperature increases, except for S6. The largest change in VTRA is calculated for S6 (1.68 ppb for 15 days of simulation), which leads to a change very similar to S5 (1.66 ppb for 15 days of simulation), where the temperature is increased by 5 degrees. The HTRA is a source term at all stations considering the surface layer, except for ATH2 and FIN. The temperature increases enhance the amount of O_3 transported to or from the station groups. On the

ACPD
11, 4355–4398, 2011

other hand, considering the entire PBL, ATH2 also becomes a receptor of O_3 transport. Contribution of HTRA is enhanced with increasing temperatures in the PBL, as it is the case for the surface layer. O_3 removal at the surface layer through HTRA increases linearly by 0.02±0.01 ppb K^{-1} over the simulation period, whereas this increase is 0.45±0.06 ppb K^{-1} in the PBL (Fig. 11b). The contribution of VTRA on O_3 is enhanced by 0.33±0.03 ppb K^{-1} at the surface layer and 0.10±0.06 ppb K^{-1} in the PBL. The largest change in DDEP is calculated for the S5 (1.84 ppb). The results point that temperature increases also enhance the dry deposition of O_3 by 0.37±0.03 ppb K^{-1} due to increases in ozone concentrations. Less O_3 is removed by CHEM when temperatures increase: a rate of −0.05±0.01 ppb K^{-1} at the surface layer and −0.72±0.10 ppb K^{-1} in the entire PBL. This suggests that chemical production of O_3 is enhanced in higher temperatures; however, destruction still dominates over production leading to a net destruction of O_3. Scenario S6 is an exception, where more O_3 is removed compared to the base case (0.04 ppb at the surface layer and 1.7 ppb in the PBL). The results indicate that the largest changes in VTRA for the 15 days of simulation occur in S6 (5.4 ppb). The responses are again linear with the temperature increases, except for S6.

Results of the IPR analyses conducted for FIN, IST and ATH1 station groups on vertical basis are also presented in Fig. 11. Overall, the figure shows that scenario S6 behaves differently with respect to budget terms of O_3 than the other scenarios. At the surface layer, the largest difference in HTRA occurs in ATH2 for scenario S6. Considering the entire PBL, the largest change is calculated at ATH1 in scenario S6. All scenarios for the other station groups show similar results for VTRA at the surface layer. Considering the surface layer, the largest differences occur at IST group, whereas within the entire PBL, FIN experiences the largest changes for VTRA. DDEP is a major sink term for all stations and scenarios, expect for S6, where the removal through dry deposition decreases compared to base case scenario. Chemistry is a major sink term in emission hot spots of IST and ATH1. At the surface layer, for both station groups, a loss of O_3 through chemistry is calculated, IST being the largest

ACPD
11, 4355–4398, 2011

affected group. On the other hand, scenario S6 leads to decreased removal of O_3 in IST. Similar pattern is seen for the PBL, where loss through chemistry increases with increasing temperatures. The production through chemistry increases in PBL for all other station groups. The circulation pattern analysis together with the IPR analyses supports the previous observation-based findings in the area that suggest the importance of transport for the air pollutant levels in the region.

4 Conclusions

The summer time O_3 concentrations and the processes governing these levels in the Eastern Mediterranean have been studied using WRF/CMAQ modeling system coupled with MEGAN model for the biogenic emission calculations for the summer in 2004. The impact of ambient temperature on O_3 concentrations and the involved processes has been investigated through temperature perturbations. The model system is able to simulate the observed isoprene concentrations at Finokalia station with an overestimation by a factor of two, which is within the uncertainty margin reported in previous studies for Europe, and better than the factor of 4 that represents an average limit of uncertainty in calculation of isoprene emissions in Europe. O_3 concentrations are also satisfactorily simulated particularly at Istanbul and Athens station groups, whereas the model performed moderately for Finokalia and Thessaloniki station groups. There is an O_3 overestimation of 48% at Finokalia station, which might be related to underestimation of dry deposition in the particular model grid cell that is largely covered by water. At other locations, the predictions overestimate the observations by 10% on average, which is acceptable given the coarse resolution of the model that results in an underestimation of O_3 titration by NO_x.

On a regional basis, the IPR results show that transport is largely responsible for the O_3 levels in the Eastern Mediterranean basin. Chemistry plays a minor role in downwind areas but is a major sink at urban cores near the surface. On the other hand, chemistry is a source term within the PBL with a more pronounced effect compared to

ACPD
11, 4355–4398, 2011

the surface layer. The IPR results point that O_3 and its precursors are carried from high altitudes and subside over the Mediterranean basin. The precursor emissions are transported away from the sources through both horizontal and vertical transport whereas they chemically destroy O_3 by reacting with NO in the urban areas. VOCs are transported away from these sources and lead to production of O_3 at downwind areas while transported. O_3 then sinks over the Mediterranean basin due to subsidence. The circulation patterns produced by the WRF model also agree with the findings of the CMAQ/IPR analyses, clearly showing the northerly transport and the subsidence over Crete. They also point to the involvement of local circulations in amplifying the impact of local emissions over the coastal urban agglomerations.

Isoprene emissions and O_3 concentrations respond almost linearly to temperature increases. The increase in ambient temperatures leads to a domain wide increase of isoprene emissions by 9±3% K^{-1}. An ozone increase of 0.9±0.1 ppb O_3 K^{-1} is calculated for the whole model domain. Simulated PAN concentrations are decreasing with increasing temperatures, which in return results in increasing NO_2 levels that produce more O_3.

Although forecasted meteorological fields would provide more realistic responses of air pollutants to changes in climate, the results of the present study clearly show that the ozone levels in the Eastern Mediterranean are subject to increase with the increasing isoprene emissions in a warmer future climate. Relatively small changes (0.9±0.1 ppb O_3 K^{-1} as computed here) might, however, contribute to summer time exceedences at the downwind areas in the Eastern Mediterranean. While developing air pollution mitigation options, possible future changes in the climate have to be taken into account.

Supplement related to this article is available online at: http://www.atmos-chem-phys-discuss.net/11/4355/2011/acpd-11-4355-2011-supplement.pdf.

ACPD
11, 4355–4398, 2011

Acknowledgements. The authors would like to acknowledge the European Union Seventh Framework Programme (FP7/2007-2013) project CityZEN (Grant Agreement no. 212095). We thank the National Air Pollution Monitoring Network of the Hellenic Ministry of Environment Energy and Climate Change for the provision of data for Athens and A. Vavatzanidis for the observational data for Thessaloniki. Regional Emissions were derived from the continental scale EMEP/INERIS inventory provided by Siour (LISA/IPSL/INERIS) and Bessagnet (INERIS). Finally, we thank G. Kouvarakis and N. Mihalopoulos for the Finokalia data and constructive discussions.

References

Athanasopoulou, E., Tombrou, M., Pandis, S. N., and Russell, A. G.: The role of sea-salt emissions and heterogeneous chemistry in the air quality of polluted coastal areas, Atmos. Chem. Phys., 8, 5755–5769, doi:10.5194/acp-8-5755-2008, 2008.

Borge, R., Alexandrov, V., del Vas, J.J., Lumbreras, J., and Rodriguez, E.: A comprehensive sensitivity analysis of the WRF model for air quality applications over the Iberian Peninsula, Atmos. Environ., 42, 8560–8574, 2008.

Byun, D. and Schere, K. L.: Review of the governing equations, computational algorithms, and other components of the Models-3 Community Multiscale Air Quality (CMAQ) modeling system, Appl. Mech. Rev., 59, 51–77, 2006.

Chen, F. and Dudhia, J.: Coupling an advanced land-surface/hydrology model with the Penn State/NCAR MM5 modeling system. Part I: model description and implementation, Mon. Weather Rev., 129, 569–585, 2001.

Crutzen, P. J.: An overview of atmospheric chemistry, European Research Course on Atmospheres (ERCA), Topics in Atmospheric and Interstellar Physics and Chemistry edited by: Boutron, C. F., 63–88, 1994.

Curci, G., Beekmann, M., Vautard, R., Smiatek, G., Steinbrecher, R., Theloke, J., and Friedrich, R.: Modelling study of the impact of isoprene and terpene biogenic emissions on European ozone levels, Atmos. Environ., 43, 1444-1455, 2009.

Dawson, J. P., Adams, P. J., and Pandis, S. N.: Sensitivity of ozone to summertime climate in the eastern USA: A modeling case study, Atmos. Environ., 41, 1494–1511, 2007.

ACPD

11, 4355–4398, 2011

Dudhia,, J.: Numerical study of convection observed during the winter monsoon experiment using a mesoscale two-dimensional model, J. Atmos. Sci., 46, 3077–3107, 1989.
ENVIRON: User's Guide CAMx-Comprehensive Air Quality Model with Extensions, Version 4.30, ENVIRON International Corporation, 415.899.0700, 2006.
Foley, K. M., Roselle, S. J., Appel, K. W., Bhave, P.V., Pleim, J.E., Otte, T. L., Mathur, R., Sarwar, G., Young, O. J., Gilliam, C. G., Kelly, J. T., Gilland, A. B., and Bash, J. O.: Incremental testing of the Community Multiscale Air Quality (CMAQ) modeling system version 4.7, Geosci. Model Dev., 3, 205–226, 2010.
Gerasopoulos, E., Kouvarakis, G., Vrekoussis, M., Kanakidou, M., and Mihalopoulos, M.: Ozone variability in the marine boundary layer of the eastern Mediterranean based on 7-year observations, J. Geophys. Res., 110, D15309, doi:10.1029/2005JD005991, 2005.
Gerasopoulos, E., Kouvarakis, G., Babasakalis, P., Vrekoussis, M., Putaud, J.-P., and Mihalopoulos, N.: Origin and variability of particulate matter (PM10) mass concentrations over the Eastern Mediterranean, Atmos. Environ., 40, 4679–4690, 2006a.
Gerasopoulos, E., Kouvarakis, G., Vrekoussis, M., Donoussis, C., Mihalapoulos, N., and Kanakidou, M.: Photochemical ozone production in the Eastern Mediterranean, Atmos. Environ., 40, 3057–3069, 2006b.
Goncalves, M., Jimenez-Guerro, P., and Baldasano, J. M.: Contribution of atmospheric processes affecting the dynamics of air pollution in South-Western Europe during a typical summertime photochemical episode, Atmos. Chem. Phys., 9, 849–864, doi:10.5194/acp-9-849-2009, 2009.
Gong, S. L.: A parameterization of sea-salt aerosol source function for sub- and super-micron particles, J. Geophys. Res., 17, 1097, doi:10.1029/2003GB002079, 2003.
Grell, G. A., Peckham, S. E., Schmitz, R., McKeen, S. A., Frost, G., Skamarock, W. C., and Eder, B.: Fully coupled "online" chemistry within the WRF model, Atmos. Environ., 39, 6957–6975, 2005.
Guenther, A., Karl, T., Harley, P., Wiedinmyer, C., Palmer, P. I., and Geron, C.: Estimates of global terrestrial isoprene emissions using MEGAN (Model of Emissions of Gases and Aerosols from Nature), Atmos. Chem. Phys., 6, 3181–3210, doi:10.5194/acp-6-3181-2006, 2006.
Hogrefe, C., Rao, S. T., Kasibhatla, P., Kallos, G., Tremback, C. J., Hao, W., Olerud, D., Xiu, A., McHenry, J., and Alapaty, K.: Evaluating the performance of regional-scale photochemical modeling systems: Part I-meteorological predictions, Atmos. Environ., 35, 4159–4174,

ACPD
11, 4355–4398, 2011

2001.
Hogrefe, C., Lynn, B., Rosenzweig, C., Goldberg, R., Civerolo, K., Ku, J.-Y., Rosenthal, J., Knowlton, K., and Kinney, P. L.: Utilizing CMAQ process analysis to understand the impacts of climate change on ozone and particulate matter, in: 4th Annual CMAS Models-3 Users' Conference, 26–28 September 2005, Chapel Hill, NC, USA, 2005.
Hong, S.-Y. and Lim, J.-O.: The WRF Single-Moment 6-Class Microphysics Scheme (WSM6), J. Korean Meteor. Soc. 42, 129–151, 2006.
Hong, S.-Y., Dudhia, J., and Chen, S.-H.: A revised approach to ice microphysical processes for the bulk parameterization of clouds and precipitation, Mon. Weather Rev., 132, 103–120, 2004.
Im, U.: Mesoscale modeling of aerosol levels in Istanbul using a high resolution MM5/CMAQ air quality modeling system, PhD Thesis, Bogazici University, Istanbul, Turkey, 2009.
Im, U., Markakis, K., Unal, A., Kindap, T., Poupkou, A., Incecik, S., Yenigun, O., Melas, D., Theodosi, C., and Mihalopoulos, N.: Study of a winter PM episode in Istanbul using high resolution WRF/CMAQ modeling system, Atmos. Environ., 44, 3085–3094, 2010.
Im, U., Poupkou, A., Incecik, S., Markakis, K., Kindap, T., Unal, A., Melas, D., Yenigun, O., Topcu, S., Odman, M.T., Tayanc, M., and Guler, M.: The impact of anthropogenic and biogenic emissions on surface ozone concentrations in Istanbul, Sci. Total Environ., doi:10.1016/j.scitotenv.2010.12.026, in press, 2011.
IPCC: Climate change 2007: Synthesis report, Intergovermental Panel on Climate Change, 2007.
Jacob, D. J. and Winner, D. A.: Effect of climate change on air quality, Atmos. Environ., 41, 51–63, 2009.
Kain, J. S.: The Kain-Fritsch convective parameterization: An update, J. Appl. Meteorol., 43, 170–181, 2004.
Kallos, G., Astitha,, M., Katsafados, P., and Spyrou, Ch.: Long-range transport of anthropogenically and naturally produced particulate matter in the Mediterranean and North Atlantic: Current state of knowledge, J. Appl. Meteorol. Climatol., 46, 1230–1251, 2007.
Kanakidou, M., Tsigaridis, K., Dentener, F. J., and Crutzen P. J.: Human-activity-enhanced formation of organic aerosols by biogenic hydrocarbon oxidation, J. Geophys. Res., 105, 9243–9254, 2000.
Kanakidou, M., Mihalopoulos, N., Kalivitis, N., Tsigaridis, K., Kouvarakis, G., Koulouri, E., Gerasopoulos, E., Vrekoussis, M., and Myriokefalitakis, S.: Natural contributions to particulate

ACPD
11, 4355–4398, 2011

matter levels over Europe – the experience from Greece, International Conference on Science and Technology (CEST) 2007, A-585–592, 2007.
Kanakidou, M., Mihalopoulos, N., Kindap, T., Im, U., Vrekoussis, M., Gerasopoulos, E., Dermitzaki, E., Unal, A., Kocak, M., Markakis, K., Melas, D., Kouvarakis, G., Youssef, A. F., Richter, A., Hatzianastassiou, N., Hilboll, A., Ebojie, F., von Savigny, C., Ladstaetter-Weissenmayer, A., Burrows, J., and Moubasher, H.: Megacities as hot spots of air pollution in the East Mediterranean. Atmos. Environ., doi:10.1016/j.atmosenv.2010.11.048, 2011.
Kindap, T., Unal, A., Chen, S. H., Hu, Y., Odman, M. T., and Karaca, M.: Long-range aerosol transport from Europe to Istanbul, Turkey, Atmos. Environ., 40, 3536–3547, 2006.
Lazaridis, M., Spyridaki, A., Solberg, S., Smolik, J., Zdimal, V., Eleftheriadis, K., Aleksanropoulou, V., Hov, O., and Georgopoulos, P. G.: Mesoscale modeling of combined aerosol and photo-oxidant processes in the Eastern Mediterranean, Atmos. Chem. Phys., 5, 927–940, 2005, http://www.atmos-chem-phys.net/5/927/2005/.
Lelieveld, J., Berresheim, H., Borrmann, S., Crutzen, P. J., Dentener, F. J., Fischer, H., Feichter, J., Flatau, P. J., Heland, J., Holzinger, R., Korrmann, R., Lawrance, M. G., Levin, Z., Markowiz, K. M., Mihalopoulos, N., Minikin, A., Ramanathan, V., de Reus, M., Roelofs, G. J., Scheeren, H. A., Sciare, J., Schlager, H., Schultz, M., Siegmund, P., Steil, B., Stephanou, E. G., Stier, P., Traub, M., Warneke, C., Williams, J., and Ziereis, H.: Global air pollution crossoads over the Mediterranean, Science, 298, 794–799, 2002.
Liakakou, E., Vrekoussis, M., Bonsang, B., Donousis, C., Kanakidou, M., and Mihalopoulos, N.: Isoprene above the Eastern Mediterranean: Seasonal variation and contribution to the oxidant capacity of the atmosphere, Atmos. Environ., 41, 1002–1010, 2007.
Liao, K.-J., Tagaris, E., Manomaiphiboon, K., Wang, C., Woo, J.-H., Amar, P., He, S., and Russel, A. G.: Quantification of the impact of climate uncertainity on regional air quality, Atmos. Chem. Phys., 9, 865–878, doi:10.5194/acp-9-865-2009, 2009.
Markakis, K., Poupkou, A., and Melas, D., Tzoumaka., P., and Petrakakis, M.: A computational approach based on GIS technology for the development of an anthropogenic emission inventory of gaseous pollutants in Greece, Water Air Soil Pollut., 207, 157–180, 2010a.
Markakis, K., Poupkou, A., and Melas, D., and Zerefos, C.: A GIS based anthropogenic PM_{10} emission inventory for Greece, Atmos. Poll. Res., 1(2), 71–81, 2010b.
Melas, D., Ziomas, I., Klemm, O., and Zerefos, C.: Anatomy of sea breeze circulation in Greater Athens under weak large-scale ambient winds, Atmos. Environ., 32, 2223–2237, 1998a.

ACPD
11, 4355–4398, 2011

Melas, D., Ziomas, I., Klemm, O., and Zerefos, C.: Flow dynamics in Athens area under moderate large-scale winds, Atmos. Environ., 32, 2209–2222, 1998b.
Melas, D., Kioutsioukis, I., and Lazaridis, M.: The impact of sea breeze on air quality in Athens, Advances in Air Pollution Modeling for Environmental Security. NATO Science Series: IV: Earth and Environmental Sciences, 54, 285–295, 2005.
Mihalopoulos, N., Stephanou, E., Kanakidou, M., Pilitsidis, S., and Bousquet, P.: Tropospheric aerosol ionic composition above the Eastern Mediterranean Area, Tellus Ser. B, 314–326, 1997.
Mlawer, E. J., Taubman, S. J., Brown, P. D., Iacono, M. J., and Clough, S. A.: Radiative transfer for inhomogeneous atmospheres: RRTM, a validated correlated-k model for the longwave, J. Geophys. Res., 102, 16663–16682, 1997.
Myriokefalitakis, S., Vrekoussis, M., Tsigaridis, K., Wittrock, F., Richter, A., Bruhl, C., Volkamer, R., Burrows, J. P., and Kanakidou, M.: The influence of natural and anthropogenic secondary sources on the glyoxal global distribution, Atmos. Chem. Phys., 8, 4965–4981, doi:10.5194/acp-8-4965-2008, 2008.
Myriokefalitakis, S., Vignati, E., Tsigaridis, K., Papadimas, C., Sciare, J., Mihalopoulos, N., Facchini, M. C., Rinaldi, M., Dentener, F. J., Ceburnis, D., Hatzianastasiou, N., O'Dowd, C., van Meele, M., and Kanakidou, M.: Global modeling of the oceanic source of organic aerosols, Adv. Meteorol., doi:10.1155/2010/939171, 2010.
Myriokefalitakis, S., Tsigaridis, K., Mihalopoulos, N., Sciare, J., Nenes, A., Segers, A., and Kanakidou, M.: In-cloud oxalate formation in the global troposphere: a 3-D modeling study, Atmos. Chem. Phys. Discuss., 11, 485–530, doi:10.5194/acpd-11-485-2011, 2011.
Odman, M. T., Hu, Y., Unal, A., Russell, A. G., and Boylan, J. W.: Determining the sources of regional haze in the Southeastern U.S. using the CMAQ model, J. Appl. Meteorol. Climatol., 46, 11, 1731–1743, 2007.
Otte, T. L. and Pleim, J. E.: The Meteorology-Chemistry Interface Processor (MCIP) for the CMAQ modeling system: updates through MCIPv3.4.1, Geosci. Model Dev., 3, 243–256, doi:10.5194/gmd-3-243-2010, 2010.
Pleim, J. E.: A combined local and nonlocal closure model for the atmospheric boundary layer. Part I: Model description and testing, J. Appl. Meteorol. Climatol., 46, 9, 1383–1395, 2007.
Poupkou, A.: Study of the photochemical air pollution over the Southeastern Europe, PhD thesis of the Aristotle University of Thessaloniki, Thessaloniki, Greece, 2006.
Poupkou, A., Symeonidis, P., Lisaridis, I., Melas, D., Ziomas, I., Yay, O. D., and Balis D.: Effects

ACPD
11, 4355–4398, 2011

of anthropogenic emission sources on maximum ozone concentrations over Greece, Atmos. Res., 89, 374–381, 2008.
Poupkou, A., Melas, D., Ziomas, I., Symeonidis, P., Lizaridis, I., Gerasopoulos, E., and Zerefos, C.: Simulated summertime regional ground-level ozone concentrations over Greece, Water Air Soil Pollut., 196, 169–181, 2009.
Poupkou, A., Giannaros, T., Markakis, K., Kioutsioukis, I., Curci, G., Melas, D., and Zerefos, C.: A model for European biogenic volatile organic compound emissions: Software development and first validation, Environ. Modell. Softw., 25, 12, 1845–1856, 2010.
Qian, Y., Gustafson Jr., W. I., and Fast, J. D.: An investigation of the sub-grid variability of trace gases and aerosols for global climate modeling, Atmos. Chem. Phys., 10, 6917–6946, doi:10.5194/acp-10-6917-2010, 2010.
San Jose, R., Perez, J. L., Pleguezuelos, C., Camacho, F., and Gonzalez, R. M.: MM5-CMAQ air quality modeling process analysis: Madrid case, Air pollution X, Ecology and the Environment vol. 53, C. A. BREBBIA, Wessex Institute of Technology, UK and University of the West of England, Bristol, UK, 2002.
Sanchez-Ccoyllo, O., Ynoue, R. Y., Martins, L. D., and Andrade, M. F.: Impacts of ozone precursor limitation and meteorological variables oz ozone concentration in Sao Paulo, Brazil, Atmos. Environ., 40, 552–562, 2006.
Seinfeld, J. H. and Pandis, S.: Atmospheric Chemistry and Physics: From Air Pollution to Climate Change, John Wiley & Sons, Inc., New York, USA, 1998.
Simpson, D., Fagerli, H., Jonson, J. E., Tsyro, S., Wind, P., and Tuovinen, J.-P.: Transboundary acidification, eutrophication and ground level ozone in Europe. PART I. Unified EMEP model description. EMEP Report 1/2003, Norwegian Meteorological Institute, ISSN 0806-4520, 104 pp., 2003.
Skamarock, W. C. and Klemp, J. B.: A time-split non-hydrostatic atmospheric model, J. Comput. Phys., 227, 3465–3485, 2008.
Sillman, S. and Samson, P. J.: Impact of temperature on oxidant photochemistry in urban, polluted rural and remote environments, J. Geophys. Res., 100(D6), 497–508, 1995.
Simpson, D., Winiwarter, W., Börjesson, G., Cinderby, S., Ferreiro, A., Guenther, A., Hewitt, N., Janson, R., Khalil, M. A. K., Owen, S., Pierce, T. E., Puxbaum, H., Shearer, M., Skiba, U., Steinbrecher, R., Tarrassón, L., and Öquist, M. G.: Inventorying emissions from nature in Europe, J. Geophys. Res., 104, 8113–8152, 1999.
Smiatek, G. and Steinbrecher, R.: Temporal and spatial variation of forest VOC emissions in

ACPD
11, 4355–4398, 2011

Germany in the decade 1994–2003, Atmos. Environ., 40, 166–177, 2006.
Steinbrecher, R., Smiatek, G., Köble, R., Seufert, G., Theloke, J., Hauff, K., Ciccioli, P., Vautard, R., and Curci, G.: Intra- and inter-annual variability of VOC emissions from natural and semi-natural vegetation in Europe and neighboring countries, Atmos. Environ., 43, 1380–1391, 2009.
Symeonidis, P., Poupkou, A., Gkantou, A., Melas, D., Yay, O. D., Pouspourika, E., and Balis, D.: Development of a computational system for estimating biogenic NMVOCs emissions based on GIS technology, Atmos. Environ., 42, 1777–1789, 2008.
Tsigaridis, K., Lathiere, J., Kanakidou, M., and Hauglustaine, D. A.: Naturally driven variability in the global secondary organic aerosol over a decade, Atmos. Chem. Phys., 5, 1891–1904, doi:10.5194/acp-5-1891-2005, 2005.
Unal, A., Hu, Y., Chang, M. E., Odman, M. T., Russel, A. G.: Airport related emissions and impacts on air quality: application to the Atlanta International Airport, Atmos. Environ. 39, 5787–5798, 2005.
Visschedijk, A. J. H., Zandveld, P. Y. J., and Denier van der Gon, H. A. C. A.: High resolution gridded European emission database for the EU Integrate Project GEMS, TNO-report 2007-A-R0233/B, 2007.
Vrekoussis, M., Mihalopoulos, N., Gerasopoulos, E., Kanakidou, M., Crutzen, P. J., and Lelieveld, J.: Two-years of NO3 radical observations in the boundary layer over the Eastern Mediterranean, Atmos. Chem. Phys., 7, 315–327, doi:10.5194/acp-7-315-2007, 2007.
Yamartino, R. J.: Nonnegative, conserved scalar transport using grid-cell-centered, spectrally constrained Blackman cubics for applications on a variable-thickness mesh, Mon. Weather Rev., 121, 753–763, 1993.
Yardwood, G., Wilson, G., Emery, C., and Guenther, A.: Development of GLOBEIS-A state of the science biogenic emissions modeling system: Final report, 1999.
Yardwood, G., Rao, S., Yocke, M., and Whitten, G. Z.: Updates to the Carbon Bond chemical mechanism: CB05. Final Report to the US EPA, RT-0400675, 8 December 2005.
Zhang, K., Knipping, E., Wexler, A., Bhave, P., and Tonnesen, G.: Size distribution of sea-salt emissions as a function of relative humidity, Atmos. Environ., 39, 3373–3379, 2005.
Zhang, Y., Vijayaraghavan, K., Huang, J., and Jacobson, M. Z.: Probing into Regional O_3 and PM Pollution: A 1-year CMAQ Simulation and Process Analysis over the United States, in: 14th Joint Conference on the Applications of Air Pollution Meteorology with the Air and Waste Management Association, 28 Janaury–2 February 2006, Atlanta, GA, USA, 2006.

ACPD
11, 4355–4398, 2011

Table 1. Air quality stations used to evaluate the model results.

Stations	Latitude (° N)	Longitude (° E)	Altitude (m a.s.l.)
		IST	
Sarachane	41.05	29.01	16
		ATH1	
Ag. Paraskevi	37.99	23.82	290
Zografou	37.97	23.79	245
		ATH2	
Liosia	38.08	23.70	165
Thrakomakedones	38.14	23.76	550
		THES	
Panaroma	40.59	23.03	363
Neochorouda	40.74	22.88	229
		FIN	
Finokalia	35.20	25.40	250

ACPD
11, 4355–4398, 2011

Table 2. Comparison of model calculated (S0) isoprene and ozone concentrations with observations for the station groups.

Parameters	Species	IST	ATH1	ATH2	THES	FIN
Correlation	Isoprene	–	–	–	–	0.5
	Ozone	0.9	0.8	0.9	0.5	0.4
Mean Normalized Bias (%)	Isoprene	–	–	–	–	90.7
	Ozone	6.1	12.2	13.5	7.1	47.5
Index of Agreement	Isoprene	–	–	–	–	0.3
	Ozone	0.9	0.7	0.7	0.6	0.4

ACPD
11, 4355–4398, 2011

Table 3. Relative per cent contributions of individual atmospheric processes to O_3, NO_x and NMVOC levels in the base case scenario (S0) for individual station group (See Table 1 for station details). HTRA stands for horizontal transport, VTRA for vertical transport, DDEP for dry deposition, CHEM for gas-phase chemistry and CLDS for cloud processes and aqueous-phase chemistry.

		Station Groups									
		IST		ATH1		ATH2		THES		FIN	
		Surface	PBL	Surface	PBL	Surface	PBL	Surface	PBL	Surface	PBL
Ozone	HTRA	6.5	27.9	15.9	49.6	−2.3	44.7	6.1	22.2	−5.4	−42.7
	VTRA	43.5	22.1	34.1	−37.2	50.0	−37.7	43.9	19.2	49.9	49.4
	DDEP	−16.2	−5.3	−34.5	−12.8	−43.4	−12.2	−48.7	−50.0	−44.4	−7.3
	CHEM	−33.8	−44.7	−15.5	0.4	−4.3	5.4	−1.3	8.7	−0.2	0.6
NO_x	HTRA	−1.1	−10.5	−0.6	−6.3	0.3	3.4	0.2	0.4	−1.4	−23.3
	VTRA	−47.8	−37.4	−47.4	−36.0	−47.9	−39.1	−47.9	−42.3	−46.4	−16.8
	DDEP	−0.9	−0.9	−0.6	−0.6	−0.7	−0.7	−1.8	−1.7	−1.5	−1.1
	CHEM	0	−0.6	−1.4	−7.1	−1.4	−10.2	−0.3	−6.0	−0.7	−8.4
	EMIS	50.0	50.0	50.0	50.0	46.7	46.6	49.8	49.6	50.0	50.0
	CLDS	−0.1	−0.5	0	0	0	0.1	0	0	0	−0.5
VOC	HTRA	−1.6	−13.4	−0.7	−8.7	0.9	5.1	0.6	2.2	0.9	5.1
	VTRA	−45.8	−33.3	−47.9	−39.7	−48.1	−47.3	−46.6	−43.3	−48.1	−47.3
	DDEP	−2.5	−2.4	−1.4	−1.4	−1.9	−1.7	−2.8	−2.6	−1.9	−1.7
	CHEM	0	−0.4	0	−0.2	−0.1	−0.9	−0.6	−4.1	0	−0.9
	EMIS	50.0	50.0	50.0	50.0	49.1	45.0	49.4	47.7	49.2	45.0
	CLDS	−0.1	−0.5	0	0	0	−0.1	0	0	0	0

ACPD
11, 4355–4398, 2011

Table 4. Domain mean changes with respect to base case simulation in response to scenarios. Emission changes are integrated over the 15-day simulation period. Concentration changes are the mean changes over the same period.

Species	Change in Scenarios					
	S1	S2	S3	S4	S5	S6
Isoprene Emissions (tons)	16.3	44.5	62.7	80.6	98.0	−7.5
Monoterpene Emissions (tons)	5.1	12.3	18.7	25.7	33.5	−0.7
Sesquiterpene Emissions (tons)	0.8	2.1	3.3	4.7	6.4	−0.2
Ozone (ppb)	1.0	1.9	2.8	3.7	4.5	0.4
NO_x (ppb)	0.1	0.1	0.1	0.1	0.1	−0.1
VOC (ppb)	0.8	1.5	1.8	2.3	2.8	−3.4

ACPD
11, 4355–4398, 2011

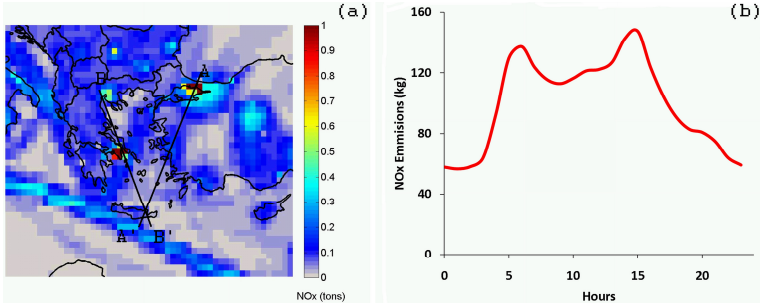

Fig. 1. NOx emissions in the model domain: **(a)** spatial distribution of emissions integrated over the 15-day simulation period (tons grid^{-1}) and **(b)** diurnal profile of emissions (kg hr^{-1}).

ACPD
11, 4355–4398, 2011

The impact of temperature changes on summer time ozone

U. Im et al.

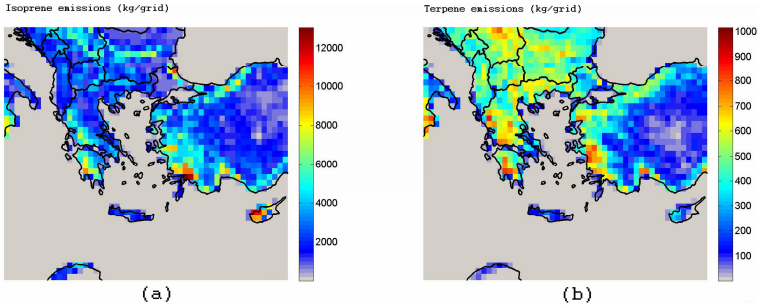

Fig. 2. (a) Isoprene and **(b)** terpene emissions (kg grid^{-1}) summed over the 15-day simulation period for the base case scenario (S0).

ACPD
11, 4355–4398, 2011

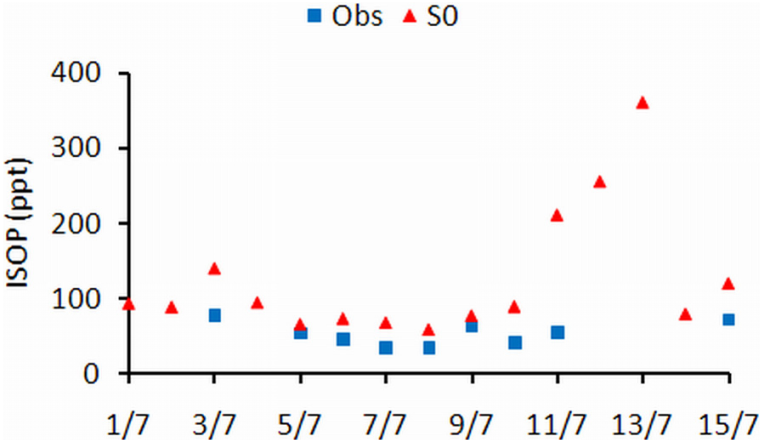

Fig. 3. Observed (squares) and modeled (triangle) daily total isoprene concentrations at Finokalia station (FIN).

ACPD
11, 4355–4398, 2011

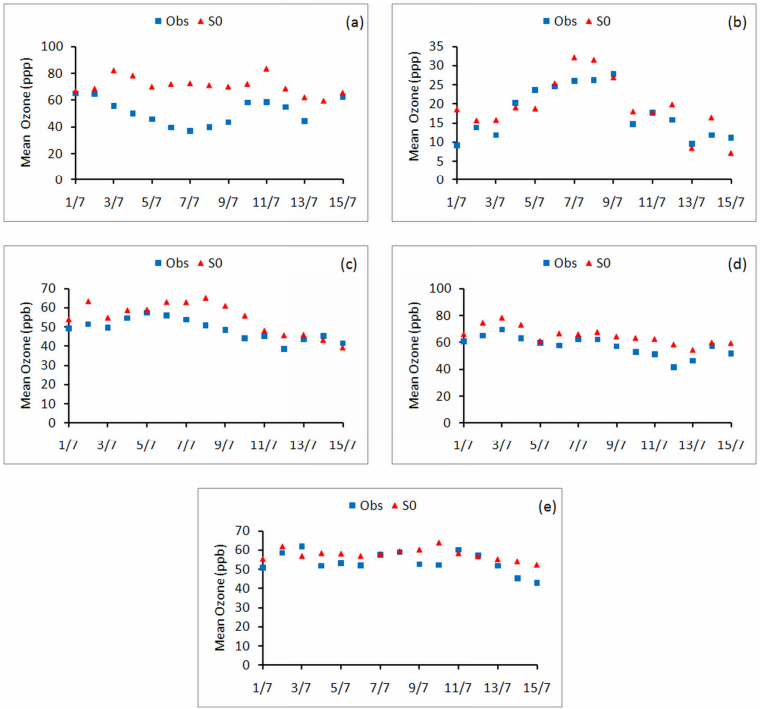

Fig. 4. Observed (square) and modeled (triangle) surface mean daily O_3 concentrations at **(a)** IST, **(b)** ATH1, **(c)** ATH2 **(d)** THES and **(e)** FIN station groups (For station details, see Table 1).

ACPD
11, 4355–4398, 2011

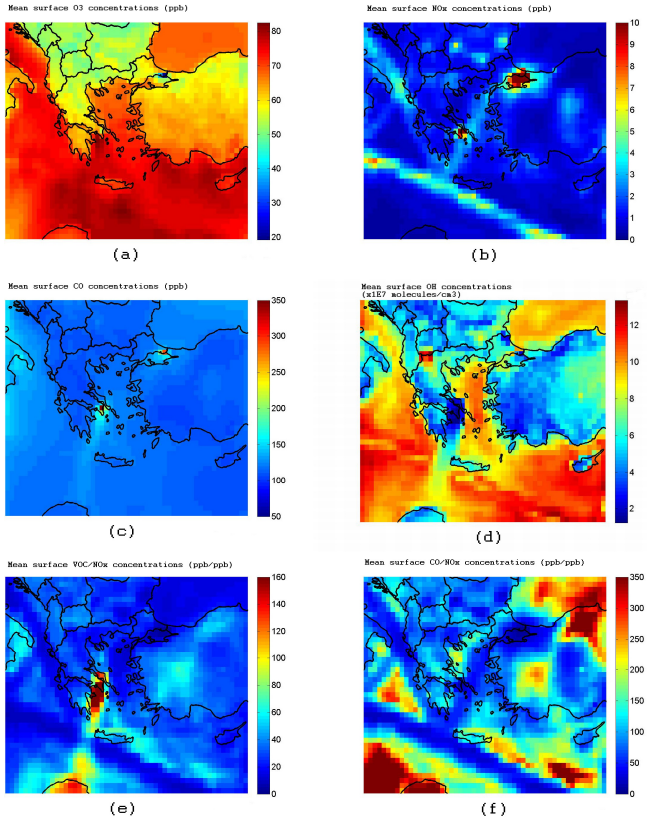

Fig. 5. Modeled distributions of mean surface **(a)** O_3, **(b)** NO_x, **(c)** CO, **(d)** OH concentrations, and **(e)** molar VOC/NO_x and **(f)** molar CO/NO_x ratios in the base case scenario (S0).

ACPD
11, 4355–4398, 2011

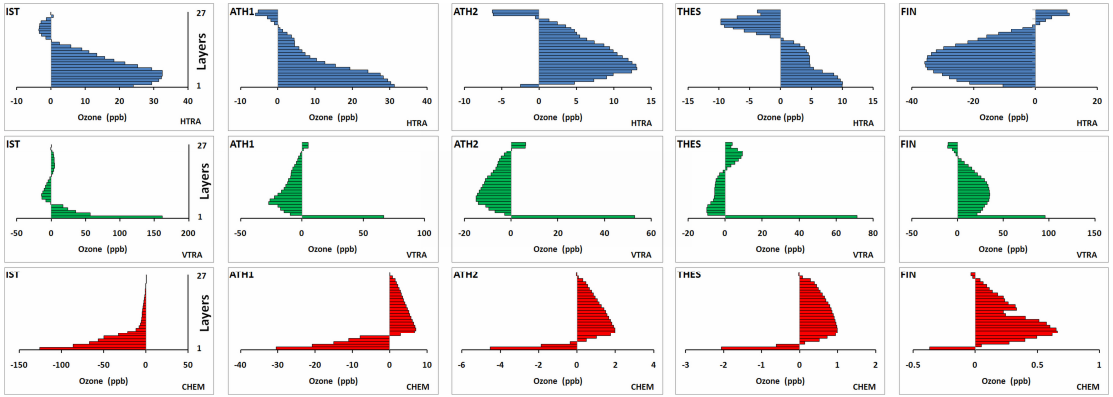

Fig. 6. Process contributions to O_3 concentrations in station groups for each vertical layer of the PBL: First row presents horizontal transport (HTRA), second row vertical transport (VTRA) and third row chemistry (CHEM). Units are ppb/15 days of simulation.

ACPD
11, 4355–4398, 2011

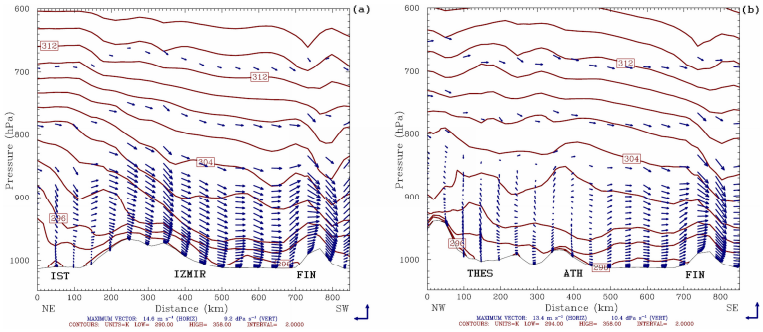

Fig. 7. Circulation vectors along **(a)** Istanbul-Finokalia (A–A′) axis and **(b)** Thessaloniki-Athens-Finokalia (B–B′) axis at 00:00 UTC, 2 July 2004.

ACPD
11, 4355–4398, 2011

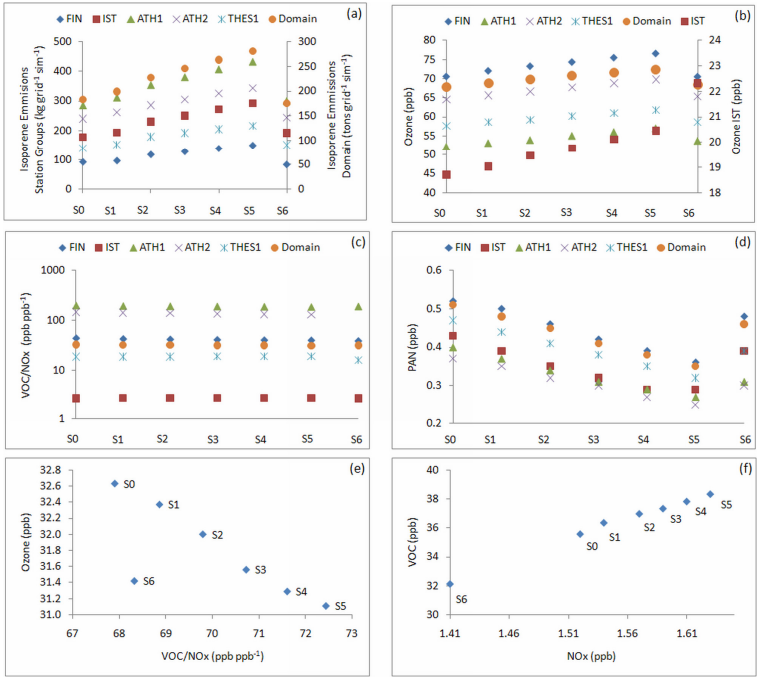

Fig. 8. Simulated **(a)** total isoprene emissions, **(b)** mean ozone, **(c)** mean molar VOC/NO_x ratio, **(d)** mean PAN, **(e)** mean molar O_3 vs. VOC/NO_x, and **(f)** mean VOC vs. NO_x for each station group and the domain; for the simulation period of 15 days.

ACPD
11, 4355–4398, 2011

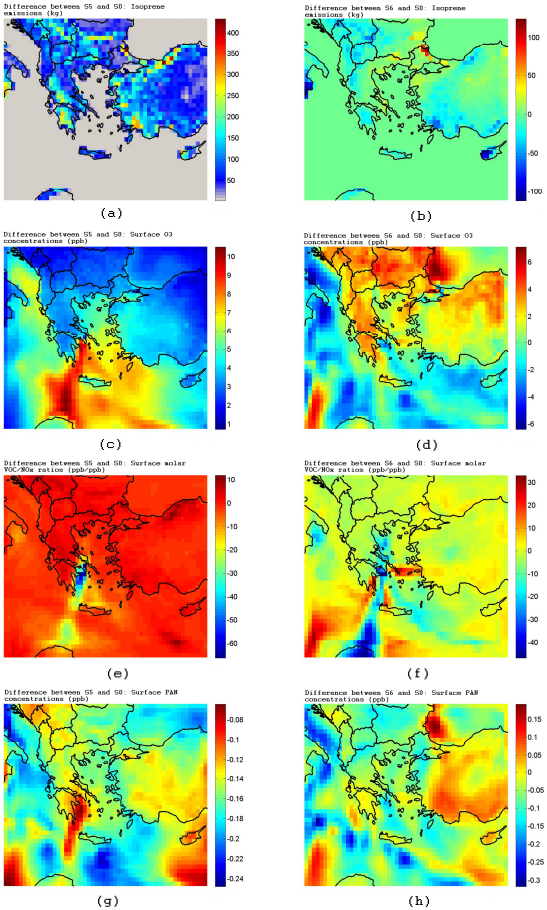

Fig. 9. Spatial differences between simulations S5 and S0 (S5-S0; left panel) and between simulations S6 and S0 (S6–S0; right panel) in: **(a, b)** isoprene emissions; **(c, d)** ozone; **(e, f)** molar VOC/NO_x ratios and **(g, h)** PAN.

ACPD
11, 4355–4398, 2011

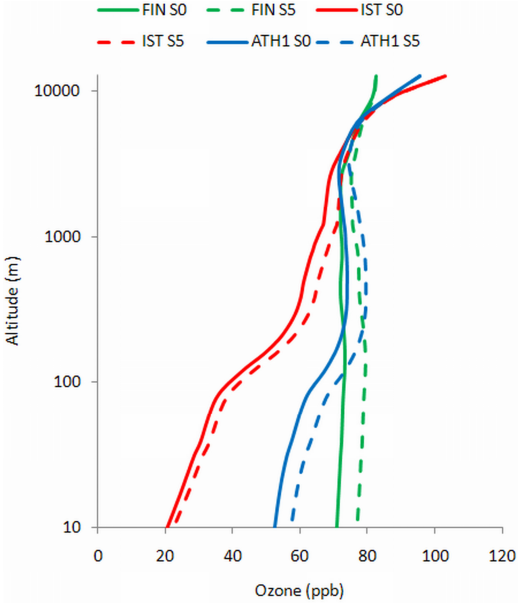

Fig. 10. Change of O_3 with altitude in base simulation (S0: solid lines) and plus 5 simulation (S5: dashed lines) for FIN, IST and ATH1 station groups for the simulation period of 15 days.

ACPD
11, 4355–4398, 2011

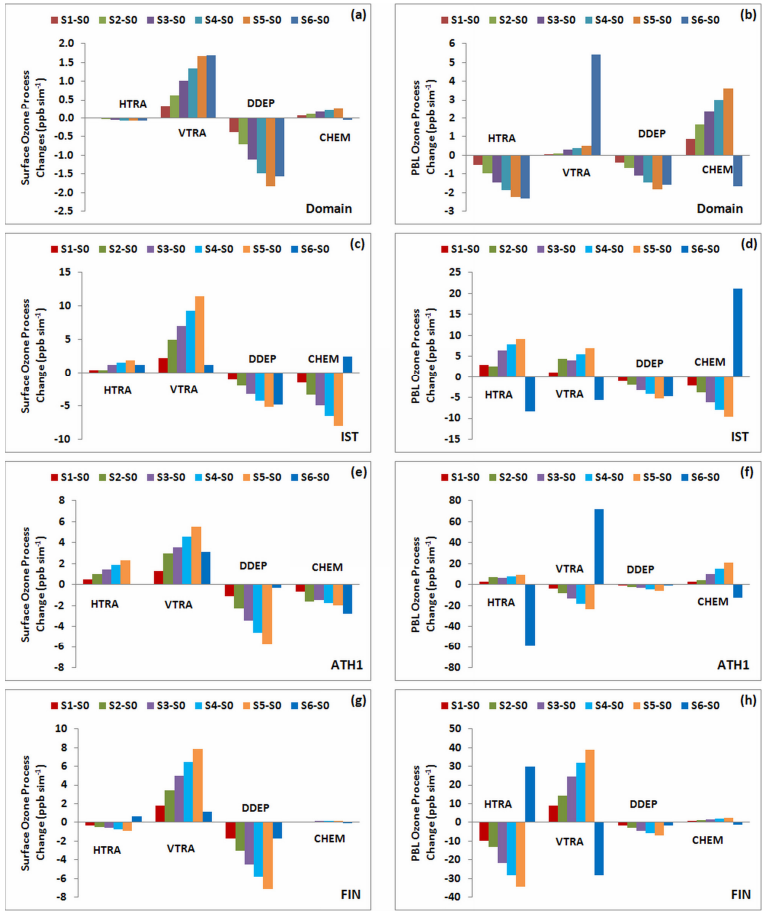

Fig. 11. Differences of mass fluxes between the perturbation simulations and the base case simulation for the surface layer (left panel) and for the entire PBL (right panel) in **(a, b)** model domain; **(c, d)** IST; **(e, f)** ATH1 and **(g, h)** FIN (units are ppb over the simulation period of 15 days).

ACPD
11, 4355–4398, 2011